Nanoscale

PAPER

View Article Online
View Journal | View Issue



Cite this: *Nanoscale*, 2016, **8**, 5771

# Facet effects of palladium nanocrystals for oxygen reduction in ionic liquids and for sensing applications†

Yongan Tang,[a] Xiaowei Chi,[a] Shouzhong Zou[b] and Xiangqun Zeng*[a]

Palladium nanocrystals enclosed by {100} and {110} crystal facets, were successfully synthesized through an aqueous one-pot synthesis method. A new thermal annealing approach was developed for fabricating these palladium nanocrystals as a working electrode on a gas permeable membrane to study the facet effects of the oxygen reduction process in an ionic liquid, 1-butyl-1-methylpyrrolidinium bis(trifluoromethylsulfonyl)imide ([Bmpy][$NTf_2$]). Results were compared with the same processes at a conventional platinum electrode. Our study shows that the structural difference between the two facets of Pd nanocrystals has little effect on the oxygen reduction process but significantly affects the oxidation process of the superoxide. It is found that the Pd{110}/IL interface can better stabilize superoxide radicals revealed by a more positive oxidation potential compared to that of Pd{100}. In addition, the analytical characteristic of utilizing both palladium nanocrystals as electrodes for oxygen sensing is comparable with a polycrystal platinum oxygen sensor, in which Pd{110} presents the best sensitivity and lowest detection limit. Our results demonstrate the facet-dependence of oxygen reduction in an ionic liquid medium and provide the fundamental information needed to guide the applications of palladium nanocrystals in electrochemical gas sensor and fuel cell research.

Received 27th October 2015,
Accepted 5th February 2016

DOI: 10.1039/c5nr07502e

www.rsc.org/nanoscale



## Introduction

Ionic liquids (ILs) have gained practical and fundamental attention as replacements of conventional electrolytes in modern electrochemical devices (*e.g.*, advanced batteries, fuel cells, super-capacitors, sensors, and electrochromic displays).[1,2] Their nonvolatile and conductive nature simplifies the design and fabrication of many electrochemical devices and their wide applied potential window enables electrochemical reactions that are not feasible in conventional solvents and electrolytes. Electrochemical gas sensors based on the measurement of changes at the electrode/electrolyte interface are among the most promising gas sensor technologies due to their properties of low cost and low power.[3–7] We have developed new gas sensor methods utilizing the unique properties of ILs and synergistically integrated them with low cost and low power electrochemical transducers that could yield forward-thinking solutions to address many gas sensor challenges, especially miniaturization and robustness.[8–10] However, the lack of fundamental understanding of the electrode/ionic interface structure presents an overarching roadblock in the IL electrochemical gas sensor development. Electrode materials are the most important factor and they often dictate the thermodynamics and kinetics of the electrode reactions which determine the sensitivity and selectivity of the gas sensor. Metal nanocrystals with controlled surface structures and high surface areas and electroactivities are ideal electrode materials for electrochemical gas sensor development. First, miniaturization of the sensor systems will often result in the miniaturization of the electrode. Metal nanocrystals provide high surface areas which can increase the sensitivity since electrochemical signals are proportional to the electrode areas. Second, sensor miniaturization requires the use of electrode materials that are compatible with microprinting and batch fabrication techniques. Nanomaterials are compatible with low cost microfabrication processes. Currently, the most studied electrode material is platinum due to its high catalytic activity for many important redox reactions such as anodic fuel oxidation as well as cathodic oxygen reduction in fuel cells. Platinum is relatively expensive compared to other noble metals. Therefore, the development of non-platinum nano electrocatalysts that have a high surface area and exhibit high catalytic activity for electrochemical reaction is an active area of research.

[a]*Department of Chemistry, Oakland University, Rochester, Michigan 48309, USA. E-mail: zeng@oakland.edu*
[b]*Department of Chemistry, American University, Washington DC 20016, USA*
†Electronic supplementary information (ESI) available: Further CV and SEM characterization of palladium nanocrystals. See DOI: 10.1039/c5nr07502e

Palladium has been investigated as a non-platinum based electrocatalyst due to its low cost and high catalytic activity for redox reactions of gas molecules.[11–13] The electrocatalytic activity of a catalyst strongly depends on the atomic arrangement of the catalyst surface.[14] The great achievement of the synthesis of nanomaterials with well-defined surface structures over the past few years has enabled the investigation of facet effects on electrochemical reactions.[15–19] The advent of well-defined palladium nanocrystals enclosed with specific facets overcomes the difficulty to fabricate palladium single crystal electrodes by Clavilier's method,[20] in which the dissolved hydrogen in palladium often bursts out from the electrode surface and destroys the crystal structure during the annealing process.[21] The catalytic activity toward oxygen reduction reaction of palladium single crystal electrodes has been investigated previously in aqueous electrolytes.[22,23] Adzic *et al.* have compared the catalytic activity of platinum monolayers deposited on Pd(111) and carbon-supported palladium nanoparticles.[24] In addition, the systematic investigation of oxygen reduction processes on different crystal planes of palladium electrodes has also been reported in aqueous solvents.[25] The catalytic activity on the low index planes of palladium was found to be completely different from that of platinum,[26] which motivates further research to provide fundamental information needed to design better Pd catalysts. In non-aqueous solvents such as ionic liquids, oxygen reduction leads to the formation of a superoxide radical anion.[27–29] It was found that the stability of the superoxide radical ($O_2^{-\bullet}$) was significantly affected by the IL cations,[30] and the effects of the IL structures and electrode materials for the redox reaction of $O_2/O_2^{-\bullet}$ were also investigated previously.[31,32] In addition, simulation of concentration profiles in ILs also confirmed that the oxygen and superoxide radical have different diffusion layer thicknesses due to the difference in the rate of diffusion, in which a large amount of superoxide radicals were accumulated near the electrode surface.[3] The affinity between the superoxide radical and IL cation is the key factor for accumulating superoxide radicals near the IL–electrode interface, which results in the different reversibility of the oxygen redox processes. Currently, there is no systematic research on the crystal facet dependence of the reaction in ILs and the facet dependence of oxygen reduction in ILs has not been studied.

We hypothesize that the facet-dependent properties of electrode materials would result in a different electrochemical process of the oxygen and superoxide radicals on the electrode surface. For example, the superoxide radical is negatively charged and the IL microenvironment will play significant roles in the accumulation of superoxide radicals in the electrode–IL interface, which will further influence the electrochemical redox process and the current signals of the $O_2/O_2^{-\bullet}$ redox process. To validate this hypothesis, we are taking advantage of the great progress in nanomaterials synthesis, in which well-defined facets of different noble metal nanocrystals have been successfully developed.[33,34] Previously, we have developed a one-pot synthesis method for synthesizing palladium cubic nanocrystals as well as five-fold twinned nanorods.[35] In this work, we further developed this method for synthesizing palladium rhombic dodecahedral (RD) nanocrystals with {110} facets at a much shorter synthesis time. We also developed a new fabrication method to fabricate nanocrystal electrodes on a gas permeable membrane. We report the first work on systematically investigated oxygen reduction reaction on both {100} and {110} facet enclosed palladium nanocrystals and compared it with that in the Pt bulk electrode to understand the facet effects of palladium toward the oxygen reduction process in an ionic liquid, 1-butyl-1-methylpyrrolidinium bis-(trifluoromethylsulfonyl)imide [Bmpy][$NTf_2$]. [Bmpy][$NTf_2$] is selected due to its high chemical and electrochemical stability in the presence of a superoxide radical,[30] which allows the systematic investigation of the facet dependent oxygen reduction in the IL. We demonstrate that the utilization of nanomaterials has great potential to increase the sensitivity of the electrochemical gas sensor and provide new ways for sensor miniaturization that are scalable.[36]

## Experimental section

$PdCl_2$ (99.999%), KI (≥99.0%), L-ascorbic acid (99%), and cetyl trimethylammonium bromide (CTAB, ≥98%) were purchased from Sigma-Aldrich. 1-Butyl-1-methylpyrrolidinium bis-(trifluoromethylsulfonyl)imide ([Bmpy][$NTf_2$], 99%) was purchased from IOLITEC Inc. A 10 mM $H_2PdCl_4$ solution was prepared by dissolving 0.0355 g $PdCl_2$ in 20 mL of 0.02 M HCl solution. Distilled water was used throughout the experiments. In a typical synthesis of rhombic dodecahedral Pd nanocrystals, 150 μL of 10 mM $H_2PdCl_4$ was added to 5 mL of 100 mM hexadecyltrimethylammonium bromide (CTAB) at 90 °C. After gently mixing the solution, 50 μL of 100 mM freshly prepared KI solution was added and the color of the solution changed from dark yellow to brown immediately. Then 200 μL of 100 mM freshly prepared L-ascorbic acid was added and the solution was kept in a 90 °C water bath for half hour. The synthesis of cubic Pd nanocrystals was the same as the dodecahedral Pd nanocrystals, except that 50 μL KI and 100 μL L-ascorbic acid were used. Scanning electron microscopy (SEM) images were acquired using a Zeiss Supra35 scanning electron microscope at 5 kV. Regular transmission electron microscopy (TEM) images and selected-area electron diffraction (SAED) images were obtained using a JEOL1200 transmission electron microscope at 120 kV.

For preparation of palladium nanocrystal electrodes, Pd nanocrystals were washed five to six times with warm water (50 °C) for removing the residual surfactants from the solution. Then a 1 to 1 ratio of water/ethanol ink solution of the nanocrystals was prepared and drop coated on a Teflon gas permeable membrane (GPM). The entire membrane was annealed at 300 °C under an ambient atmosphere for removing the surfactants and immobilizing the nanocrystals on the membrane surface. Since both the electrode area and catalytic activity contribute to the current signal of the redox reaction, the nanocrystal electrode surface area needs to be carefully

 

quantified to systematically compare how different facets of the nanocrystal affect the electrode reactions. Briefly the electrochemically active surface area was measured with a redox probe of 0.01 M ferrocene in the IL at various scan rates. Based on the Randles–Sevcik equation ($i_p = 268\,600n^{3/2}AD^{1/2}Cv^{1/2}$), the redox reaction of ferrocene/ferrocenium can be used for obtaining the relationship between the peak current and surface area, as shown in Fig. S1 (ESI†). The diffusion coefficient of ferrocene in [Bmpy][$NTf_2$] was obtained by using a CHI Pt electrode, in which the initial surface area was calculated by hydrogen adsorption/desorption charges (210 μC $cm^{-2}$) in 0.1 M $HClO_4$.

A Clark-type electrochemical gas cell was used in this study similar to our previous paper.[37] Platinum gauze (Sigma-Aldrich) was used as a polycrystalline platinum working electrode for comparison of oxygen sensing performance. All electrochemical measurements were performed on a CHI 1000A electrochemical workstation (CH Instrument, Inc.). Two 0.5 mm-diameter platinum wires were used as the counter and quasi-reference electrode respectively. All of the potential reported was converted and referenced *versus* ferrocene unless specifically mentioned. The total gas flow rate was maintained at 200 sccm by digital mass-flow controllers (MKS Instruments, Inc.) and the volume ratio (v/v)% of oxygen to nitrogen was adjusted by two mass-flow controllers.

## Results and discussion

### Fabrication and characterization of palladium nanocrystal electrode

Fig. 1 shows the scanning electron microscopy images of palladium nanocrystals. Fig. 1A shows the SEM image of orderly arranged cubic palladium nanocrystals squarely assembled on a silicon substrate. Fig. 1B shows the selected area electron diffraction (SAED) pattern of a cubic palladium nanocrystal (inset is the TEM image). The square pattern confirms the {100} facet of cubic palladium nanocrystals. The self-assembled tetragonal superlattice structure of cubic palladium nanocrystals in Fig. 1A indicates the high uniformity in size and shape of the synthesized cubic nanocrystals. Fig. 1C shows the SEM image of orderly arranged rhombic dodecahedral (RD) palladium nanocrystals. The elongated hexagon SAED pattern in Fig. 1D also confirms the {110} enclosed facets of the prepared RD palladium nanocrystals. The high quality of palladium nanocrystals enabled the accurate investigation of the facet-dependence of oxygen reduction reaction.

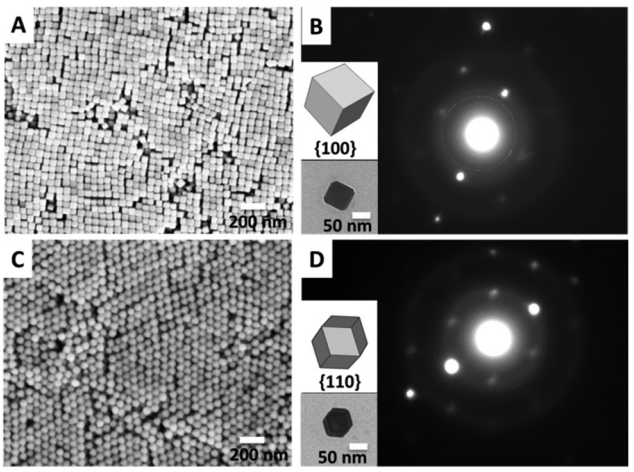


Fig. 1 SEM images of orderly assembled (A) cubic (C) rhombic dodecahedral (RD) Pd nanocrystals; (B) SAED pattern of cubic Pd nanocrystal (inset: schematic structure and corresponding TEM image of a cubic Pd nanocrystal), (D) SAED pattern of RD Pd nanocrystal (inset: schematic structure and corresponding TEM image of a RD Pd nanocrystal).

Due to the high viscosity of ILs, the study of the electrochemical oxygen reduction process in ILs requires the use of a Clark type of electrochemical cell with a porous PTFE Teflon gas permeable membrane (GMP). Gas analytes entering from the GMP side can quickly reach the electrode/electrolyte interface without passing through the IL diffusion barrier. Typical of a Clark cell, the working electrode is made of a sputtered or evaporated metal layer deposited directly onto a GPM and worked as the sensing cathode. One important issue in the application of nanomaterials as the electrode is the immobilization of nanocrystal catalysts in addition to the surfactant removal from nanoparticles. In order to immobilize the nanocrystals on the membrane, they were drop-coated on the membrane and annealed at 300 °C under an ambient atmosphere. The thermal annealing process for nanomaterials has been shown to effectively remove surfactants from the nanoparticles for obtaining a clean catalyst surface.[38,39] No obvious size or morphology change was observed for the nanocrystals annealed in this process, as shown by the SEM image of the annealed RD and cubic palladium nanocrystals in Fig. S2 (ESI†). The unchanged morphology of palladium nanocrystals enables the accurate facet-dependent measurement for oxygen detection using the Clark type of electrochemical cell. In addition, the immobilized palladium nanocrystals show very good adhesive characteristics on the membrane surface which is critical for their utility as the working electrode in a sensor. We further used an electrochemical approach to validate the facets of palladium nanocrystals coated on the GPM. Different crystal facets of palladium will present different electrochemical features of surface oxidation and hydrogen adsorption/desorption due to different surface atomic arrangements in aqueous electrolytes.[40] The cyclic voltammograms of Pd{100} and Pd{110} after the annealing process are presented in Fig. S3 (ESI†). Hydrogen desorption peaks were observed at a more positive potential on Pd{100} (+0.2 V) compared to Pd {110} (+0.1 V), which is consistent with the reported electrochemical feature of palladium nanocrystals.[16] The oxidation of Pd{110} at 0.7 V also showed a much larger current density that is consistent with bulk palladium single crystal electrodes (*vs.* RHE). These electrochemical results combined with the SEM images confirmed the preservation of the specific facets ({100} and {110}) on the palladium nanocrystals after they are fabricated on the GPM.

### Pd facet effects on oxygen reduction in [Bmpy][NTf$_2$]

In aqueous media, the oxygen reduction reaction has been investigated thoroughly due to its importance in many applications such as fuel cells. Oxygen can be reduced to either $H_2O_2$ or $H_2O$ *via* two- or four-electron reduction pathways with the formation of oxygen-containing species, such as O, OH, and OOH.[40,41] These intermediates might have different binding affinity facets that will block or alter the adsorption of oxygen. Therefore, information on the facet-dependence for ORR in aqueous media is a combination of the facet effect on oxygen and the intermediate. In contrast, electrochemical reduction of oxygen in different ILs follows a simple one-electron transfer mechanism and produces a superoxide radical as the final product.[42–44]

$$O_2 + e^- \rightarrow O_2^{-\bullet} \quad (1)$$

Carter *et al.* first reported the superoxide radical formation that is not stable resulting in irreversible voltammetry features of one-electron oxygen reduction in room temperature molten salts.[45] Later partially reversible voltammograms and stabilization of superoxide radicals were reported in imidazolium ILs.[46] The superoxide radical forms strong ion-pairing ([cation]$^+\cdots O_2^{-\bullet}$) in imidazolium ILs, which is the reason for the irreversible voltammograms and more positive oxidation potential of superoxide radicals.[47] An oxygen sensor based on the above reaction has been developed for detecting oxygen by using a polycrystalline platinum electrode.[4] The activity of an electrochemical reaction often strongly depends on the atomic arrangement of the electrode surface. The structurally well-defined palladium nanocrystals provide the opportunity for studying the facet effects on the oxygen reduction processes in ILs which has not been studied before.

The influence of different IL electrolytes with different cations but the same anion has been studied in our previous work and the stability of the ions of IL toward superoxide radicals is shown to be important for their long term stability and reversibility.[30] [Bmpy][NTf$_2$] was shown to be the most stable IL towards a superoxide radical and is selected for the palladium nanocrystal electrode study. Cyclic voltammetry was used to characterize oxygen reduction on different facets of palladium nanocrystals, as shown in Fig. 2. Similar to the conventional platinum bulk electrodes, the redox peaks of the $O_2$/$O_2^{-\bullet}$ couple present an asymmetrical shape (I/II and I′/II′ peaks) due to the specific interaction between the $O_2^{-\bullet}$ and cations of the IL, in which a typical steady-state characteristic is presented.[48,49] In imidazolium based ILs, superoxide radicals tend to form a strong ion pair with the imidazolium cation ([Im]$^+$) because of their negative charge and delocalized electronic spin density.[50] The oxygen reduction potential for palladium nanocrystals are both at −1.1 V, so the structural facet difference among two palladium nanocrystals does not result in the potential difference in oxygen reduction reaction on palladium. The oxygen reduction on Pd{110} (Fig. 2B, peak I′) shows broad peak features and higher current density compared with Pd{100} (Fig. 2A, peak I), which might indicate

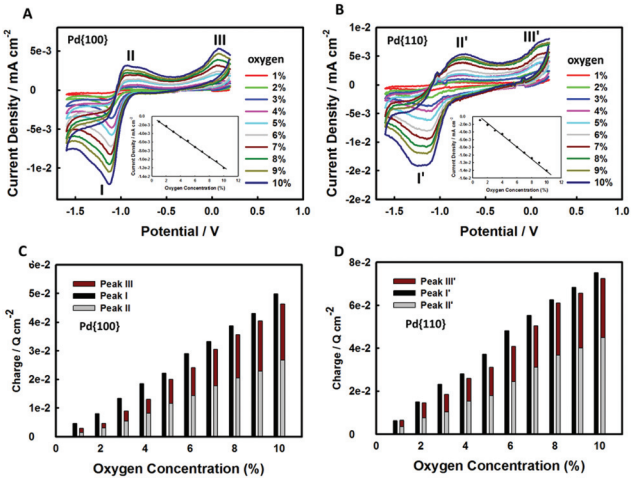


Fig. 2 Cyclic voltammograms of Pd nanocrystals in [Bmpy][NTf$_2$] with different concentrations of oxygen (1%–10% v/v) (A) cubic nanocrystals (B) RD nanocrystals, inset: calibration curve of peak current at I and IV (third cycle). Scan rate: 0.1 V s$^{-1}$ (C) and (D) charge plots of peaks obtained in (A) and (B), respectively.

more active sites for oxygen reduction on the Pd{110} surface. Furthermore, the reduction peak potential of Pd nanocrystals is more positive than that of platinum (−1.2 V, Fig. S4, ESI†) which confirms the higher catalytic activity of Pd nanocrystals than that of Pt. One important electrochemical feature between the two facets of palladium nanocrystals is the oxidation potential of the superoxide radical. It is found that the oxidation potential of the superoxide radical on Pd{110} (peak II′) is at −0.75 V, which is 200 mV more positive than that on Pd{100} (peak II, −0.95 V). Since the same IL electrolyte was used in both palladium nanocrystal electrodes, the difference in oxidation potential should be due to the facet difference of palladium nanocrystals. As mentioned above, a more positive oxidation potential of superoxide radicals indicates a stronger affinity between the superoxide radical anion and the IL cation which made it harder to be oxidized when studied on the same electrode material but with different ILs. The same IL is used in the current study, thus the IL–electrode interface should contribute to the stabilization of the superoxide radical. This is the first time that information on facet-dependence for superoxide radical oxidation, which can serve as the first step to understand the electrochemical behavior of an $O_2$/$O_2^{-\bullet}$ redox couple in ILs at nanocrystal electrodes, has been provided.

For face-centered cubic lattice metals such as palladium, the first layer atomic densities of three low-index planes decrease in the order of {111} > {100} > {110},[51] and the surface energies of these three low-index facets increase in the reverse order (1.31, 1.49, 1.55 J m$^{-2}$).[52] Different facets can present different molecular adsorption properties due to the distance variation between crystal atoms.[53–55] The more open atomic arrangement of {110} provides more step sites that may benefit the catalytic activity of palladium toward oxygen reduction as well as the stabilization of superoxide radicals.

 

Another possible explanation is based on the different affinity of the cations on different Pd facets since the electrode potential is quiet negative during the oxygen reduction process. The electrochemical quartz crystal microbalance (EQCM) study shows that carbon dioxide anion radicals adsorb at a highly negative potential,[28] which suggests that the affinity of superoxide radical is more important in this observed facet selectivity. Interestingly, the trend of higher catalytic activities of Pd{110} *vs.* Pd{100} toward oxygen reduction is different from that obtained on bulk Pd single crystal electrodes in acidic aqueous solutions, where Pd{100} shows the highest ORR activity.[26] The difference may arise from the different reactions in aqueous *vs.* IL media. Fig. S5 (ESI†) shows the peak current of oxygen reduction and superoxide radical oxidation *vs.* scan rate results from these two types of palladium nanocrystals. It is found that the reduction peak current of oxygen (peak I and I′) and the oxidation peak current of the superoxide radical (peak II and II′) both presented a linear relationship with the square root of scan rate, which indicates a diffusion controlled process of the oxygen redox process.

The oxygen reduction process in both Pd {110} and {100} in [Bmpy][$NTf_2$] is much less reversible than that observed at the Au electrode.[30] As shown in Fig. 2C and D, the charge of oxidation of the superoxide radical is only around 50% compared to the charge of oxygen reduction in both Pd{100} and Pd {110}. An additional oxidation peak at 0.1 V was observed for both palladium nanocrystals in [Bmpy][$NTf_2$]. This peak is only observed in an imidazolium based IL at the Au electrode since the ion-pairing of $[Im]^+\cdots O_2^{-\bullet}$ facilitates the protonation of the superoxide radical to form hydroperoxide and a new species of dehydrogenated IL cation at the Au electrode.[56,57] This oxidation peak was assigned to the oxidation of hydroperoxide anions and is attributed to the stability of the cation of an IL toward superoxide radicals.[30] Our results suggest that at palladium nanocrystal electrodes, the cation of [Bmpy][$NTf_2$] is less stable toward the superoxide radical than that at Au with the following possible reactions:

$$O_2^{-\bullet} - e^- \rightarrow O_2 \text{ [peak (II/II′)]} \quad (2)$$

$$[Bmpy]^+ \cdots O_2^{-\bullet} \rightarrow [Bmpy]_{de}^+ + HO_2^- \quad (3)$$

$$[Bmpy]_{de}^+ + HO_2^- - e^- \rightarrow [Bmpy]^+ + O_2 \text{ [peak (III/III′)]} \quad (4)$$

Eqn (2) denotes the superoxide radical oxidation (peak II and II′) that is the reverse process of oxygen reduction (eqn (1)). Eqn (3) represents the pronation process of the ion pair structure between the IL cation and the superoxide radical; possible pronated structures of the IL cation $[Bmpy]_{de}^+$ are listed in Table S1.† Eqn (4) is an irreversible reaction since no corresponding reduction partners for peak III and peak III′ are presented in Fig. 2A and B respectively. The charge analysis of the CV curves in the oxygen reduction process supports the above interpretation since the total oxidation charge of peak III and III′ (eqn (4)) and superoxide radicals (peak II and II′) are almost equal to the reduction charge of oxygen (peak I and I′) without the consideration of the loss of the superoxide radical due to diffusion and decomposition. But a small difference between Pd {110} and Pd {100} is also observed as shown in Fig. 2C and D. At low oxygen concentration (1–2%, v/v) when the loss of superoxide radicals due to diffusion was minimum, the oxidation charge is almost identical to the reduction charge (Fig. 2D) on Pd{110}. However, on Pd{100} the total charge for oxidation and reduction is still different at low oxygen concentration (1–2%, v/v). This suggests the lower stabilization of the superoxide radical to Pd{100} compared to Pd{110}. Fig. S6 (ESI†) summarizes the charge ratio of the oxygen redox process. It is found that the ratio of the related peaks on Pd{110} *vs.* Pd{100} always shows a value larger than one, which indicates the higher catalytic activity of Pd{110}. For the oxidation processes (peaks II/II′ or III/III′), an even larger value compared to the reduction process (I/I′) was observed, which indicated that the Pd{110} facet shows higher activity for the superoxide oxidation process than that of the Pd{100} facet. Thus, these results further confirm the conclusion that Pd{110} facets can stabilize superoxide radicals better than that of Pd{100}. The inset calibration curves of Fig. 2A and B show linear relationships between the oxygen reduction current (peak I and I′) and concentration on both the palladium nanocrystal electrodes. The less negative reduction potential of oxygen on palladium electrodes *vs.* platinum and the high stabilization of the superoxide radical anion on the Pd{110} nanocrystal surface should benefit the IL based electrochemical oxygen sensor development based on oxygen reduction in ILs.

## Amperometric oxygen sensor using palladium nanocrystal electrodes

Among different electrochemical techniques, amperometry has been widely used to identify and quantify electroactive species.[58] When a sufficiently negative potential was applied, the current ($i$) obtained from chronoamperometry should come from two contributions. One was the Faradaic current from oxygen reduction ($i_f$) that followed the Cottrell equation ($i_f = nFACD^{1/2}\pi^{-1/2}t^{-1/2}$); the other was the double layer charging current ($i_d$). Since the charging current decayed much faster (exponential function) than the Faradaic current (square root of time for a diffusion-controlled reaction), the current from double layer charging normally considered as insignificant when current is sampled at a time exceeding $3R_sC_d$ ($R_s$ is the solution resistance and $C_d$ is the double layer capacitance. $R_sC_d$ is called the time constant). Here, the initial measurement of oxygen began at a time exceeding $3R_sC_d$, in which the charging current can be considered negligible as the signal only contributed from the Faraday current. Two types of palladium nanocrystal electrodes were first tested in low concentration oxygen (1%–5%, v/v) sensing for validating the feasibility of using palladium nanocrystals as the oxygen sensing electrodes.

Fig. 3A shows the baseline adjusted current density response of the IL-based amperometric sensor for Pd nano-

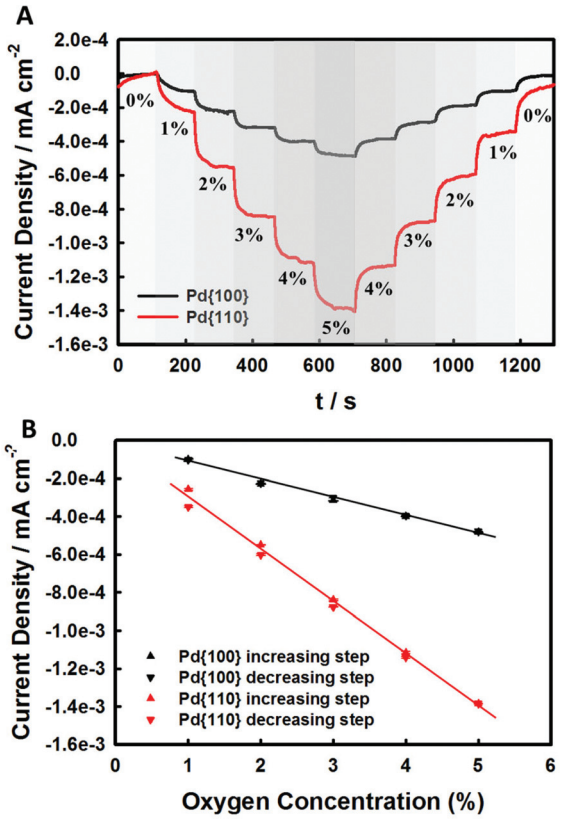


Fig. 3 (A) Current density *vs.* time plot for Pd nanocrystal in different oxygen concentration (1%–5%, v/v), (potential: −1.1 V). (B) Calibration curves for oxygen sensing on Pd nanocrystal electrodes obtained in A.

crystal electrodes at oxygen concentrations from 1% to 5%. The current was normalized to the respective electrochemically active surface area of Pd nanocrystals. The applied potential for palladium nanocrystal electrodes was at −1.1 V as indicated in Fig. 2. The holding time at each oxygen concentration was 100 seconds before increasing the concentration for the next measurement. Plots of calibration derived from data in Fig. 3A are linear in the five different concentrations tested, as shown in Fig. 3B. It is found that the sensitivity of Pd{110} is much higher than that of Pd{100} and is an order of magnitude higher than that reported previously for a sensor based on the hydrophilic IL at the gold electrode,[59] which confirmed the benefits and feasibility of using Pd nanocrystal electrodes for oxygen sensor development. The potential applied for oxygen sensing on the palladium electrode is −1.1 V which is less negative than platinum (−1.2 V). There are additional benefits of using palladium as the electrode material for oxygen sensors in view of energy and cost. In addition, the facet-dependent results suggest that new nanocrystals with different facets can be studied to change the electrode reaction activity. Since ionic liquids are promising sensor electrolytes, the facet-dependent sensor performance here would provide insights into their applications in developing robust IL-based electrochemical sensors.

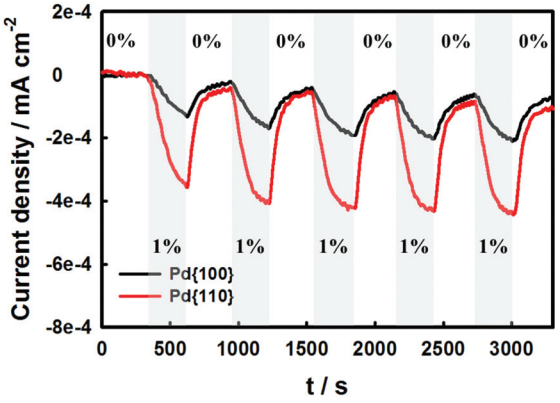


Fig. 4 Constant-potential current response measured over five cycles of alternate exposure to 1% (v/v) oxygen.

In order to further validate the reversibility of palladium nanocrystals for oxygen sensors, repeated measurements at a specific oxygen concentration (1% v/v) were performed, as shown in Fig. 4. Both Pd{100} and Pd{110} electrodes show good reversibility toward oxygen sensing, characterized by completely reversible and reproducible value and returned to the baseline under pure nitrogen flow (0% oxygen). The Pd{100} and Pd{110} based sensors toward 1% (v/v) oxygen have an average sensitivity of −0.136 μA cm$^{-2}$ and −0.317 μA cm$^{-2}$, with standard deviation of 14.4 nA cm$^{-2}$ and 17.2 nA cm$^{-2}$ respectively. Sensors present a slight drift on the baseline due to the change of the double layer capacitor charging current. The larger baseline drift of Pd{110} shown in Fig. 4 can be attributed to the higher stabilization of the superoxide radical compared to Pd{100}, which has been validated by cyclic voltammetry in Fig. 2. The stronger stabilization of the superoxide radical for Pd{110} led to superoxide radical accumulation near the electrode surface and caused the larger baseline drift compared to Pd{100}. The mechanistic understanding of oxygen reduction at two Pd nanocrystal facets can guide further development of baseline correction methods.

$$j\ (\mu\text{A cm}^{-2}) = -0.288C_{O_2\%} - 0.303 \quad (R^2 = 0.997)\ (\text{Pd}\{110\}) \tag{5}$$

$$j\ (\mu\text{A cm}^{-2}) = -0.171C_{O_2\%} - 0.154 \quad (R^2 = 0.997)\ (\text{Pd}\{100\}) \tag{6}$$

$$j\ (\mu\text{A cm}^{-2}) = -0.187C_{O_2\%} - 0.279 \quad (R^2 = 0.996)\ (\text{Pt polycrystal}) \tag{7}$$

Practical applications require an analytical method for detection in a wide concentration range of oxygen. A wide concentration range of oxygen (1%–20% v/v) was tested with these sensors together with the conventional polycrystal Pt electrode sensor for comparison, as shown in Fig. 5A. The current density was normalized to the electrochemically active area of the electrode for signal comparison between sensors. Three measurements in each oxygen concentration (six times for 1% oxygen) were recorded in order to obtain an accurate value and

 

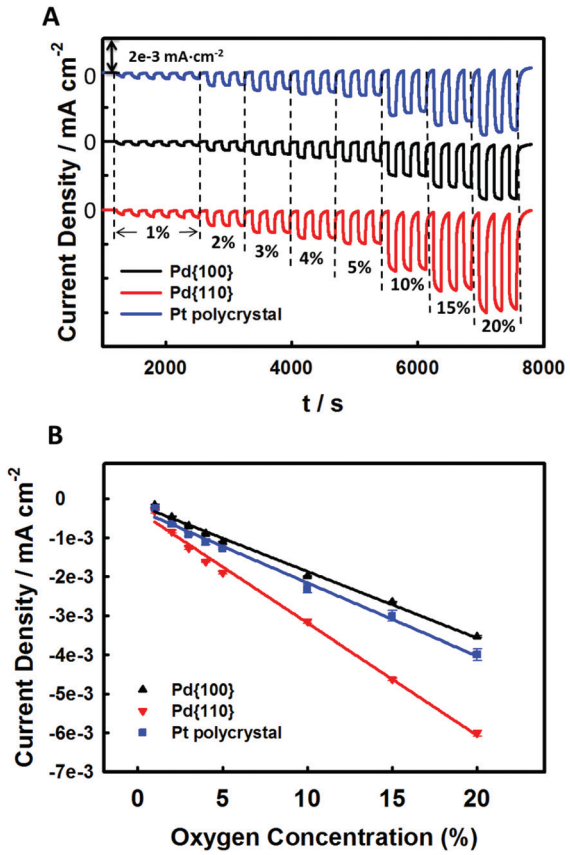


**Fig. 5** (A) Current density *vs.* time plot for Pd nanocrystals and Pt polycrystal in different oxygen concentration (1%–20% v/v). (Potential: −1.2 V for platinum, −1.1 V for palladium), (B) calibration curves for three different electrodes in A.

standard deviation of the sensor signal response. The potential for the Pt polycrystal electrode was selected at −1.2 V based on the CV results presented in Fig. S4 (ESI†), while the potential for palladium nanocrystal electrodes was maintained at −1.1 V. A two minute interval for oxygen on/off duration time was selected for the measurement. The calibration curves for three sensors are plotted in Fig. 5B. All of the three sensors presented a linear relationship between the oxygen concentration and current signal response, and their linear equations are shown in eqn (5)–(7). As seen in these equations, the Pd{100} electrode exhibits similar sensitivity to polycrystalline Pt, and the Pd{110} electrode shows about 2 times higher sensitivity than that of Pt or Pd{100}. Table 1 summarizes the figures of merit in these calibration curves for the three types of electrodes.

**Table 1** Figures of merit for three different electrodes in oxygen detection

| | $S_{bl}$ ($\mu A \cdot cm^{-2}$) | DL ($C_{O_2\%}$) | Linear range (v/v) | Sensitivity ($\mu A \cdot cm^{-2}\ \%^{-1}$) |
|---|---|---|---|---|
| Pt polycrystal | $1.910 \times 10^{-3}$ | 0.031 | 1–20% | −0.187 |
| Pd {100} | $4.650 \times 10^{-4}$ | 0.008 | 1–20% | −0.171 |
| Pd {110} | $3.360 \times 10^{-4}$ | 0.004 | 1–20% | −0.288 |

The detection limits (DL) were calculated from three times the standard deviation of the blank signal ($S_{bl}$). Palladium nanocrystal based sensors present a much lower detection limit compared with the platinum polycrystal electrode, which confirmed that it is suitable and superior as the working electrode in sensor application.

## Conclusion

In this paper, a new one-pot synthesis method was developed for synthesizing {110} and {100} facet enclosed palladium nanocrystals. These nanocrystals were successfully fabricated onto a gas permeable membrane surface and act as the working electrode materials for studying oxygen reduction reactions. The surface properties of the fabricated nanocrystal sensor remain unchanged and enable the fundamental facet-dependent investigation of the electrochemical properties of oxygen reduction and superoxide radical oxidation. It is found that different facets of palladium nanocrystals exert little effect on the oxygen reduction process but affect the oxidation process of the superoxide radical significantly. The results show that the Pd{110}facet has stronger interactions with superoxide radicals and present more positive oxidation potential than that of Pd{100}. This is the first time the facet-dependent properties for the oxygen/superoxide radical in an ionic liquid solvent, which provide the fundamental facet information for designing better sensor electrodes, have been reported.

In addition, oxygen sensing was characterized by using Pd nanocrystals which validated the benefits and feasibility of palladium nanocrystals as the working electrode for oxygen sensing in a wide dynamic concentration range (1%–20%) in IL *vs.* Pt. The palladium nanocrystal offered advantage in oxygen sensing by lowering the reduction potential and increasing the sensitivity compared to the polycrystalline platinum electrode. The results for the two types of palladium nanocrystals ({110} and {100}) indicate that the oxygen reduction occurring on the palladium surface was affected by the surface atom orientation, in which the higher surface energy facet of {110} has better catalytic activity for oxygen reduction. This result is different from the catalytic activity sequence of oxygen reduction reaction in aqueous solvent. The difference is attributed to the different electrochemical processes of oxygen reduction, in which only one electron transfer process occurred when an ionic liquid was used as the electrolyte compared to the two- or four-electron transfer process in aqueous solvents. Therefore, the unique redox mechanisms in ionic liquids together with their facet-dependent properties of electrode materials should provide an opportunity for combining the advantage of nanomaterials and ionic liquids for practical sensor application.

## Acknowledgements

X. Zeng would like to acknowledge support from NIOSH R01OH009644-01A1 and NIEHS R01ES022302 for this work.

## Notes and references


1 A. Rehman and X. Zeng, *RSC Adv.*, 2015, **5**, 58371–58392.
2 D. R. Macfarlane, M. Forsyth, P. C. Howlett, J. M. Pringle, J. Sun, G. Annat, W. Neil and E. I. Izgorodina, *Acc. Chem. Res.*, 2007, **40**, 1165–1173.
3 D. S. Silvester and R. G. Compton, *Z. Phys. Chem.*, 2006, **220**, 1247–1274.
4 Z. Wang, P. Lin, G. A. Baker, J. Stetter and X. Zeng, *Anal. Chem.*, 2011, **83**, 7066–7073.
5 X. Mu, Z. Wang, X. Zeng and A. J. Mason, *IEEE Sens. J.*, 2013, **13**, 3976–3981.
6 J. Liu, S. Wagan, M. D. Morris, J. Taylor and R. J. White, *Anal. Chem.*, 2014, **86**, 11417–11424.
7 J. Liu, M. D. Morris, F. C. Macazo, L. R. Schoukroun-Barnes and R. J. White, *J. Electrochem. Soc.*, 2014, **161**, H301–H313.
8 A. Rehman and X. Zeng, *Acc. Chem. Res.*, 2012, **45**, 1667–1677.
9 Z. Wang, M. Guo, G. A. Baker, J. R. Stetter, L. Lin, A. J. Mason and X. Zeng, *Analyst*, 2014, **139**, 5140–5147.
10 Y. Tang, Z. Wang, X. Chi, M. D. Sevilla and X. Zeng, *J. Phys. Chem. C*, 2016, **120**(2), 1004–1012.
11 Y. T. Lee, J. Lee, H. Hwang, H. Jung, W. Lee, H. Bae and S. Im, *Sens. Actuators, B*, 2015, **209**, 490–495.
12 F. Favier, E. C. Walter, M. P. Zach, T. Benter and R. M. Penner, *Science*, 2001, **293**, 2227–2231.
13 Y. J. Lu, J. Li, J. Han, H. T. Ng, C. Binder, C. Partridge and M. Meyyappan, *Chem. Phys. Lett.*, 2004, **391**, 344–348.
14 S. Ye, T. Kondo, N. Hoshi, J. Inukai, S. Yoshimoto, M. Osawa and K. Itaya, *Electrochemistry*, 2009, **77**, 2–20.
15 I. Esparbe, E. Brillas, F. Centellas, J. A. Garrido, R. M. Rodriguez, C. Arias and P. L. Cabot, *J. Power Sources*, 2009, **190**, 201–209.
16 H. X. Zhang, H. Wang, Y. S. Re and W. B. Cai, *Chem. Commun.*, 2012, **48**, 8362–8364.
17 Y. Xiong and Y. Xia, *Adv. Mater.*, 2007, **19**, 3385–3391.
18 Y. Xiong, J. M. McLellan, Y. Yin and Y. Xia, *Angew. Chem., Int. Ed.*, 2007, **46**, 790–794.
19 Y. J. Xiong, J. M. McLellan, J. Y. Chen, Y. D. Yin, Z. Y. Li and Y. N. Xia, *J. Am. Chem. Soc.*, 2005, **127**, 17118–17127.
20 J. Clavilier, R. Faure, G. Guinet and R. Durand, *J. Electroanal. Chem.*, 1980, **107**, 205–209.
21 N. Hoshi, K. Kagaya and Y. Hori, *J. Electroanal. Chem.*, 2000, **485**, 55–60.
22 V. Mazumder, Y. Lee and S. Sun, *Adv. Funct. Mater.*, 2010, **20**, 1224–1231.
23 T. J. Schmidt, V. Stamenkovic, M. Arenz, N. M. Markovic and P. N. Ross, *Electrochim. Acta*, 2002, **47**, 3765–3776.
24 J. Zhang, Y. Mo, M. B. Vukmirovic, R. Klie, K. Sasaki and R. R. Adzic, *J. Phys. Chem. B*, 2004, **108**, 10955–10964.
25 M. Shao, T. Yu, J. H. Odell, M. Jin and Y. Xia, *Chem. Commun.*, 2011, **47**, 6566–6568.
26 S. Kondo, M. Nakamura, N. Maki and N. Hoshi, *J. Phys. Chem. C*, 2009, **113**, 12625–12628.
27 K. U. Schwenke, J. Herranz, H. A. Gasteiger and M. Plana, *J. Electrochem. Soc.*, 2015, **162**, A905–A914.
28 C. Xiao and X. Zeng, *J. Electrochem. Soc.*, 2013, **160**, H749–H756.
29 V. S. Bryantsev, V. Giordani, W. Walker, M. Blanco, S. Zecevic, K. Sasaki, J. Uddin, D. Addison and G. V. Chase, *J. Phys. Chem. A*, 2011, **115**, 12399–12409.
30 C. Xiao, A. Rehman and X. Zeng, *RSC Adv.*, 2015, **5**, 31826–31836.
31 S. Ernst, L. Aldous and R. G. Compton, *J. Electroanal. Chem.*, 2011, **663**, 108–112.
32 R. G. Evans, O. V. Klymenko, S. A. Saddoughi, C. Hardacre and R. G. Compton, *J. Phys. Chem. B*, 2004, **108**, 7878–7886.
33 H. Z. Yang, Y. G. Tang and S. Z. Zou, *Electrochem. Commun.*, 2014, **38**, 134–137.
34 W. X. Niu, L. Zhang and G. B. Xu, *ACS Nano*, 2010, **4**, 1987–1996.
35 Y. A. Tang, R. E. Edelmann and S. Z. Zou, *Nanoscale*, 2014, **6**, 5630–5633.
36 I. Grunwald, E. Groth, I. Wirth, J. Schumacher, M. Maiwald, V. Zoellmer and M. Busse, *Biofabrication*, 2010, 2.
37 Z. Wang and X. Zeng, *J. Electrochem. Soc.*, 2013, **160**, H604–H611.
38 D. Li, C. Wang, D. Tripkovic, S. Sun, N. M. Markovic and V. R. Stamenkovic, *ACS Catal.*, 2012, **2**, 1358–1362.
39 Z. Liu, M. Shamsuzzoha, E. T. Ada, W. M. Reichert and D. E. Nikles, *J. Power Sources*, 2007, **164**, 472–480.
40 N. Hoshi, M. Nakamura, N. Maki, S. Yamaguchi and A. Kitajima, *J. Electroanal. Chem.*, 2008, **624**, 134–138.
41 A. M. Bond and B. S. Grabaric, *Anal. Chem.*, 1979, **51**, 337–341.
42 C. Zhao, A. M. Bond, R. G. Compton, A. M. O'Mahony and E. I. Rogers, *Anal. Chem.*, 2010, **82**, 3856–3861.
43 M. E. Ortiz, L. J. Nunez-Vergara and J. A. Squella, *J. Electroanal. Chem.*, 2003, **549**, 157–160.
44 A. S. Barnes, E. I. Rogers, I. Streeter, L. Aldous, C. Hardacre, G. G. Wildgoose and R. G. Compton, *J. Phys. Chem. C*, 2008, **112**, 13709–13715.
45 M. T. Carter, C. L. Hussey, S. K. D. Strubinger and R. A. Osteryoung, *Inorg. Chem.*, 1991, **30**, 1149–1151.
46 I. M. AlNashef, M. L. Leonard, M. C. Kittle, M. A. Matthews and J. W. Weidner, *Electrochem. Solid-State Lett.*, 2001, **4**, D16–D18.
47 C. A. Brooks and A. P. Doherty, *J. Phys. Chem. B*, 2005, **109**, 6276–6279.
48 M. Hayyan, F. S. Mjalli, I. M. AlNashef and M. A. Hashim, *Int. J. Electrochem. Sci.*, 2012, **7**, 9658–9667.
49 M. Hayyan, F. S. Mjalli, M. A. Hashim and I. M. AlNashef, *Ind. Eng. Chem. Res.*, 2012, **51**, 10546–10556.
50 E. I. Rogers, X.-J. Huang, E. J. F. Dickinson, C. Hardacre and R. G. Compton, *J. Phys. Chem. C*, 2009, **113**, 17811–17823.
51 L. Vitos, A. V. Ruban, H. L. Skriver and J. Kollar, *Surf. Sci.*, 1998, **411**, 186–202.
52 N. E. Singh-Miller and N. Marzari, *Phys. Rev. B: Condens. Matter*, 2009, 80.
53 Y. G. Tang, J. W. Yan, F. Zhu, C. F. Sun and B. W. Mao, *Langmuir*, 2011, **27**, 943–947.


 

54 J. W. Yan, Y. G. Tang, C. F. Sun, Y. Z. Su and B. W. Mao, *Langmuir*, 2010, **26**, 3829–3834.
55 Y. A. Tang, J. W. Yan, X. S. Zhou, Y. C. Fu and B. W. Mao, *Langmuir*, 2008, **24**, 13245–13249.
56 M. M. Islam, T. Imase, T. Okajima, M. Takahashi, Y. Niikura, N. Kawashima, Y. Nakamura and T. Ohsaka, *J. Phys. Chem. A*, 2009, **113**, 912–916.
57 I. M. AlNashef, M. A. Hashim, F. S. Mjalli, M. Q. A.-h. Ali and M. Hayyan, *Tetrahedron Lett.*, 2010, **51**, 1976–1978.
58 J. R. Stetter and J. Li, *Chem. Rev.*, 2008, **108**, 352–366.
59 M. C. Buzzeo, O. V. Klymenko, J. D. Wadhawan, C. Hardacre, K. R. Seddon and R. G. Compton, *J. Phys. Chem. A*, 2003, **107**, 8872–8878.